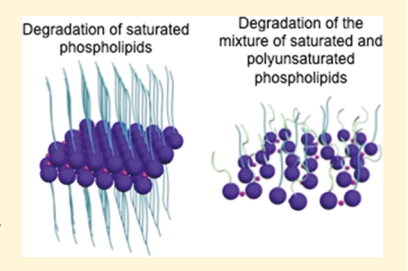
LANGMUIR © Cite This: Langmuir 2019, 35, 11643–11650

Polyunsaturated Phospholipid Modified Membrane Degradation Catalyzed by a Secreted Phospholipase A2

Pin Zhang,[†] Veronica Villanueva,[†] Joseph Kalkowski,[†] Chang Liu,[†] Tiep Pham,[†] Ursula Perez-Salas,[‡] Wei Bu,[§] Binhua Lin,[§] and Ying Liu*,[†]

Supporting Information

ABSTRACT: To optimize the compositions of the lipid-based nanomedicine and to advance understanding of the roles of polyunsaturated phospholipids in biological membranes, this study examined the effects of polyunsaturated phospholipids on the degradation of giant unilamellar vesicles catalyzed by a secreted phospholipase A2 (sPLA₂) using fluorescence microscopy. Molecular interfacial packing, interaction, and degradation of the films containing various mixing ratios of saturated and polyunsaturated phospholipids were quantified using a Langmuir trough integrated with synchrotron X-ray surface scattering techniques. It was found that a high molar fraction (0.63 and above) of polyunsaturated phospholipids not only enhanced the rate of sPLA2-catalyzed vesicle



degradation but also changed the vesicle deformation process and degradation product morphology. Hydrolysis of the saturated phospholipids generated highly ordered liquid crystal domains, which was reduced or prohibited by the presence of the polyunsaturated phospholipids in the reactant film.

INTRODUCTION

Phospholipids predominant in most biological membranes have at least one unsaturated bond in their alkyl tails. Polyunsaturated phospholipids are those with two or more double bonds in at least one alkyl tail, which are abundant in membranes of the nervous system and retina. 1-3 Phospholipase A2 (PLA₂) is a superfamily of enzymes that catalyze the hydrolysis of sn-glycero-3-phospholipids, generating equimolar lysophospholipids and fatty acids. Secreted PLA2 (sPLA2) is one of the major categories of PLA2 and is widely present in the venoms of insects and reptiles and in the tissues of mammals.4-6 sPLA2 plays important roles in membrane remodeling, lipid regulation, and cell signaling,6 and its dysregulation has been related to a variety of diseases, ^{7,8} such as inflammatory diseases ⁹ and cancers. ^{10,11} To date, most research on sPLA2 has been focused on the enzyme-catalyzed degradation of saturated phospholipids. A few studies have examined the degradation of monounsaturated phospholipids (with only one double bond in at least one alkyl tail) catalyzed by sPLA2, finding that inclusion of monounsaturated phospholipids increased membrane fluidity and reduced the degradation latency time of sPLA2. 12,13 Most studies on polyunsaturated phospholipids are based on detection of their functions in cell membrane regulation, such as increasing membrane disorder and fluidity, 14-17 promoting vesicle fission and enhancing cell endocytosis, facilitating formation of lateral domains on membranes, and modulating membrane protein functions. 18-20 Although effects of polyunsaturated phospholipids on membrane properties and degradation may be qualitatively extrapolated from the studies of monounsaturated phospholipids, the common presence of polyunsaturated phospholipids in biological processes suggests that polyunsaturation has unique functions and quantification of their effects on molecular packing and interaction is necessary.

Furthermore, sPLA₂-catalyzed degradation of phospholipids with sn-2 polyunsaturated alkyl chains generates polyunsaturated fatty acids, which are crucial in many physiological processes and in modulation and prevention of diseases.^{21,22} For example, docosahexaenoic acid helps the brain to maintain its structures and functions,²³ and arachidonic acid (AA) is involved in cell signaling and important in defending against inflammatory diseases. ^{24–26} However, molecular interactions of polyunsaturated lipids with $sPLA_2$ have rarely been systematically investigated. Therefore, the need to understand its role in related physiological and pathological processes gives impetus to the quantitative investigation of the degradation of polyunsaturated phospholipids catalyzed by sPLA₂.

The intrinsic level of sPLA₂ related to certain diseases can be exploited for diagnostic purposes and as therapeutic strategies for treating these diseases.⁵ Intrinsic sPLA₂ overexpressed in diseases (such as inflammation diseases and several types of cancer) may be employed as a trigger to facilitate the targeted release of drugs from lipid-based drug delivery systems, increasing drug efficacy and reducing side effects. ^{27–29} To achieve the goal of rapid release in the target areas, many current designs of liposomes contain negatively charged lipids

Received: May 17, 2019 Revised: August 5, 2019 Published: August 12, 2019

[†]Department of Chemical Engineering and [‡]Department of Physics, University of Illinois at Chicago, Chicago, Illinois 60607, United

[§]NSF's ChemMatCARS, University of Chicago, Chicago, Illinois 60637, United States

that have been reported to enhance liposome degradation catalyzed by several sPLA₂ isoforms. However, negatively charged liposomes may also activate the complement system and reduce liposome circulation time.^{30,31} An alternative method is to include unsaturated phospholipids in membranes to increase fluidity and enhance degradation.^{32,33} Compared to monounsaturated phospholipids, polyunsaturated phospholipids exhibited stronger disturbance of lipid membrane structures and greater enhancement of the catalytic activity of sPLA₂.³⁴ However, their applications in drug delivery systems have not been systematically explored.

In this study, 1,2-dipalmitoyl-sn-glycero-3-phosphocholine (DPPC) and 1,2-dilinoleoyl-sn-glycero-3-phosphocholine (DLPC) were employed as model saturated and polyunsaturated phospholipids. Molecular structures and hydrolysis of DPPC and DLPC are presented in Figure S1 of the Supporting Information. DPPC, a saturated phospholipid, has been intensively used as a substrate in different lipid assemblies to study the catalyzed activity of sPLA₂. ³⁵⁻⁴¹ DLPC has two *cis*carbon double bonds in each tail. One of its degradation products—linoleic acid (LA)—is a polyunsaturated omega-6 fatty acid, one of the two essential fatty acids for human health and one of the main sources for biosynthesis of AA. ⁴²

In the present work, evolution of giant unilamellar vesicles (GUVs) consisting of DPPC and DPPC–DLPC mixtures upon addition of sPLA₂ was monitored under fluorescence microscopy. X-ray reflectivity (XR), which provides information on molecular organization across the interface, and grazing-incidence X-ray diffraction (GIXD), which reveals the two-dimensional crystal structures at the interface, were applied to characterize the interfacial structures of the monolayers before and after sPLA₂-catalyzed degradation.

MATERIALS AND METHODS

Materials and Reagents. DPPC, DLPC, and 1,2-dipalmitoyl-sn-glycero-3-phosphoethanolamine-N-(lissamine rhodamine B sulfonyl) (ammonium salt) (DPPE–Rhod, Ex/Em 560/583 nm) were purchased from Avanti Polar Lipids. Palmitic acid (PA, ≥99%), LA (≥99%), sPLA₂ from honey bee venom (Apis mellifera), calcium chloride dihydrate, hydrochloric acid, organic solvents (including acetonitrile, chloroform, ethanol, and methanol), and indium tin oxide (ITO)-coated glass slides (25 mm × 25 mm × 1.1 mm) with a surface resistivity of 8 to 12 Ω /sq were purchased from Sigma-Aldrich. Tris base was purchased from Fisher. Water used in all experiments was deionized to 18.2 MΩ (MILLIPORE). All chemicals were used as received.

GUV Preparation. The phospholipids were dissolved in chloroform with 5 vol % acetonitrile at a 5 mM lipid concentration and stored at -20 °C. The phospholipid mixtures contained 0.5 mol % DPPE-Rhod to provide a fluorescent contrast. GUVs were generated based on a modified electroformation method. 43-45 Specifically, a thin uniform coating of phospholipids was prepared on an ITO-coated glass slide by spreading 200 μ L of phospholipid solution on the conducting side of the ITO-coated glass slide and then spinning the glass slide at 600 rpm for 4 min (Laurell Technologies). The residue solvent was removed by placing the lipid-coated glass slide in an oven with nitrogen at 50 °C for 2 h. A chamber was formed by placing another ITO glass slide over the lipid-coated ITO glass slide separated by an O-ring (ID 0.614 in. and OD 0.754 in., McMaster-Carr) (Supporting Information, Figure S2). The chamber was filled with degassed 0.5 mM Tris buffer, which was preheated to 50 °C. Subsequently, a 1 V, 10 Hz ac field was added to this chamber for 1.5 h at 50 °C. After electroformation, the GUV samples were maintained in the sealed chamber at 50 °C for 30 min and then gently collected using a glass pipette.

Observation of GUV Degradation Catalyzed by sPLA2. For imaging, 10 μ L of the GUV suspension was placed on a glass slide and observed using an epifluorescence microscope (Zeiss Observer, D1-AX10). The incident light was provided by an X-Cite series 120 Q bulb with a TEXAS RED filter (Ex/Em 565/620 nm). For GUV degradation, 20 μ L of a solution of sPLA2 in 0.15 mM CaCl2 and 0.5 mM Tris buffer was added to the GUV suspensions at various sPLA2 concentrations. The mixture was immediately pipetted back and forth a few times to ensure homogeneous mixing. GUV degradation was recorded for 15 min by an AxioCam MRm camera (Zeiss) with a 40× air objective (LD Plan-NEOFLUAR 40×). The temperature of the sample stage was maintained at 23 °C by a Linkam controller during the measurements.

Quantification of Molecular Packing at the Gas-Liquid Interface. Characterization of the molecular packing structures of lipid films at the gas-liquid interface was done using XR and Measurements were performed at the National Science Foundation's ChemMatCARS (15-IDC beamline) at the Advanced Photon Source user facility of Argonne National Laboratory. The Xray wavelength was 1.24 Å. The lipid films were formed on a customized Langmuir trough (78 × 177.6 mm) with a single barrier and a subphase stirring system. The trough was enclosed in a gas-tight box. The interfacial tension was measured by a Wilhelmy plate (paper) hooked to a wire that was attached to an electronic balance (KSV NIMA, Biolin Scientific). X-ray data were collected by a Pilatus 100 K area detector. All experiments were conducted at a controlled temperature of approximately 22.7 °C. Before each experiment, the trough was cleaned and filled with 65 mL of buffer solution (5 mM CaCl₂ 8 mM Tris pH 7.4). The cleanliness of the surface was verified by monitoring the surface pressure whose fluctuation should be less than 0.2 mN m⁻¹ during the entire change of the surface area. After 20 μ L of a freshly prepared lipid solution was spread at the gas-liquid interface, the gas-tight box containing the trough was immediately sealed and purged with helium gas until the oxygen concentration inside the box was less than 1%. The surface pressure-mean molecular area isotherms of the lipid monolayers were monitored during the compression until the monolayers collapsed.

For the X-ray measurements, the films were compressed by the barrier at a rate of 5 cm² min $^{-1}$ until the surface pressure reached a target value of either 25 or 10 mN m $^{-1}$. After completion of both XR and GIXD measurements on the lipid films, the barrier position was fixed to keep the surface area constant. With a quick action, the box was opened to inject 32.5 μ L of 20 μ g mL $^{-1}$ sPLA $_2$ solution into the subphase, the final concentration of sPLA $_2$ in the subphase was 10 ng mL $^{-1}$. The box was then resealed and purged with helium. The subphase was gently stirred for 1 h to achieve a homogeneous distribution of the enzyme. An additional hour was allowed for film degradation to reach a quasi-equilibrium state. XR and GIXD measurements were then conducted on the degraded films at a constant surface area.

Model Fitting of X-ray Data. XR measures the electron density profile $\rho(z)$ produced by the lipid film across the gas—liquid interface. The intensity of the reflected X-rays is measured as a function of the scattering vector normal to the interface: Q_{σ} given by $(4\pi \sin\theta)/\lambda$, where θ is the angle of incidence relative to the surface and λ is the X-ray wavelength. The normalized X-ray reflectivity was obtained through dividing the reflected intensity R by the Fresnel reflectivity $R_{\rm F}$ produced by the ideal flat bare gas—liquid interface. The normalized X-ray reflectivity was fitted using a box model to describe the electron density profile of the lipid film as follows 49

$$\rho(z) = \frac{1}{2} \sum_{i=0}^{N} \operatorname{erf}\left(\frac{z - z_i}{\sqrt{2} \times \sigma}\right) \times (\rho_i - \rho_{i+1}) + \frac{\rho_0}{2}$$
(1)

where ρ_i is the electron density of the ith slab, ρ_0 is the electron density of the subphase, N is the number of slabs needed to describe the lipid film across the interface (N=2 in our models), and z_i is the position of the ith interface. A smooth varying electron density transition between consecutive slabs is represented by a sum of the error functions in which σ is the overall roughness of the film.

GIXD was presented as a function of both horizontal wave vector Q_{xy} (parallel to the interface) and vertical wave vector $Q_{z}^{47,48}$. Integrating the intensities over the entire Q_{z} range of the two-dimensional GIXD curves produced Bragg peaks, which were fitted using Gaussian functions to reveal the two-dimensional lattice structures of the molecules at the interface. By integrating the intensity over Q_{xy} , Bragg rods were obtained. The Bragg rods were then fitted using the distorted wave Born approximation (DWBA), and information on the tilting angle of the ordered molecules was obtained.

RESULTS AND DISCUSSION

GUV Degradation Kinetics and Morphology Changes. Including polyunsaturated phospholipids in the membranes not only enhanced the vesicle degradation rates but also changed the deformation phenomena and degradation product morphology. Typical images of the degradation evolution of DPPC and DPPC–DLPC GUVs (with a DLPC fraction of $x_{\rm DLPC} = 0.63$) at two different concentrations of sPLA₂ are presented in Figure 1. At a low sPLA₂ concentration (0.1 μ g

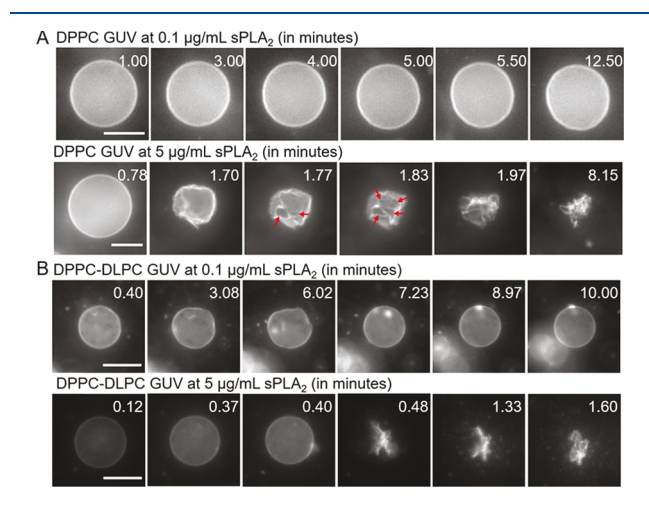


Figure 1. Images of DPPC and DPPC–DLPC GUVs during their degradation upon mixing with sPLA₂ at 23 °C. (A) Evolution sequences of DPPC GUVs after mixing with 0.1 μg mL⁻¹ sPLA₂ (top row) and 5 μg mL⁻¹ sPLA₂ (bottom row), representing typical types of GUV degradation. The red arrows point to defects formed on the membrane. (B) Evolution sequences of DPPC–DLPC GUVs (with a DLPC fraction of $x_{\rm DLPC}=0.63$) after mixing with sPLA₂ at 0.1 (top row) and 5 μg mL⁻¹ (bottom row), representing typical types of vesicle degradation. The time (in minute) after mixing with sPLA₂ is displayed in the upper right corner of each frame. The scale bar in all frames is 20 μ m. Exposure times were autoadjusted to provide the best contrast. Details of the imaging process are presented in Table S1 of the Supporting Information.

mL⁻¹), the DPPC GUVs retained their size and morphology (top row of Figure 1A). When the sPLA₂ concentration was increased 50-fold (to 5 μ g mL⁻¹), many GUVs shrank and membrane defects with well-defined boundaries and sharp corners (indicated by the red arrows) appeared on the membranes (bottom row of Figure 1A). The vesicles then further decayed to bright, crystal-like clusters, which were likely to be the highly ordered PA–Ca²⁺ complexes.⁵¹

Degradation of DPPC–DLPC GUVs in the presence of sPLA₂ was found to be different from those of DPPC GUVs. DPPC–DLPC GUVs attained a transient irregular shape when exposed to a low sPLA₂ concentration (0.1 μ g mL⁻¹) but relaxed back to the original spherical shape (top row of Figure

1B). At a 50-fold higher enzyme concentration, most of the DPPC-DLPC GUVs quickly burst to form bright aggregates and small dots (bottom row of Figure 1B). However, these bright aggregates were unlikely crystal structures, as no obvious line-structure or sharp edges were detected as those in DPPC GUVs. The control experiments were conducted under the same conditions except the absence of the enzyme, which ruled out the possibility of significant size or morphology change in GUVs due to osmotic pressure (Figure S3 of the Supporting Information).

Upon addition of sPLA₂, the degradation path was dictated by the kinetics of enzyme adsorption and lipid degradation (reaction kinetics) followed by the transport kinetics of the reaction products into the solution and the molecular reorganization within the membrane. At a low enzyme concentration, the reaction was slow, having little effect on the shape of the vesicles. However, at a high enzyme concentration, the fast reactions and quick loss of lysophospholipids from the GUVs resulted in shrinking or bursting of the GUVs. Polyunsaturated phospholipids affected the degradation process in two ways: (1) polyunsaturated phospholipids packed loosely, allowing the enzyme to adsorb more readily and resulting in faster vesicle degradation, and (2) degradation products of the polyunsaturated phospholipids disrupted crystal structure formation.

Multiple GUVs were observed and statistically analyzed. The difference between degradation of DPPC–DLPC GUVs and DPPC GUVs became clearer in a comparison of the statistical distribution of the observed conditions for the same elapsed time, as a function of sPLA2 concentrations (Figure 2). The correlation between the degradation kinetics and sPLA2 concentration was nonlinear, as the concentrations of sPLA2 were plotted as individual conditions instead of on a linear scale (Figure 2). In comparison to DPPC GUVs, the DPPC–DLPC GUVs required a lower concentration of sPLA2 to achieve a high proportion of structurally deformed vesicles at the same elapsed time. Figure 2 shows not only a different distribution of degradation results between the two types of GUVs but also different degradation phenomena.

Quantification of Interfacial Organization of Lipid Monolayers at the Gas-Liquid Interface. In order to understand at the molecular level how polyunsaturated phospholipids affected lipid packing in mixed membranes of DPPC and DLPC and how lipid packing in turn affected the way in which sPLA2 catalyzed their degradation, we studied representative lipid monolayer films at the gas-lipid interface. Surface pressure-mean molecular area isotherms of monolayers of DPPC, DLPC, and mixtures of DPPC and DLPC $(x_{\text{DLPC}} = 0.2, 0.4, \text{ and } 0.63)$ at the gas-liquid interface are presented in Figure 3A. When compressed, the DPPC film transitioned from a liquid-expanded (LE) phase to a coexistence state of liquid-expanded and condensed (LE-C) phases. Upon further compression, the LE-C phase transitioned to a single condensed (C) phase.⁵³ Introducing DLPC in the monolayer produced more fluid films, as the monolayer compression isotherm curves shifted to a larger mean molecular area at the same surface pressures, the span of the LE phase became significantly broader, and the LE-C coexistence region occurred at higher surface pressures. When the molar fraction of DLPC was 0.63 or higher, the films collapsed before reaching the condensed phase. The shifting of isotherms to a higher mean molecular area and the disappearance of the LE-C transition phase resulting from the

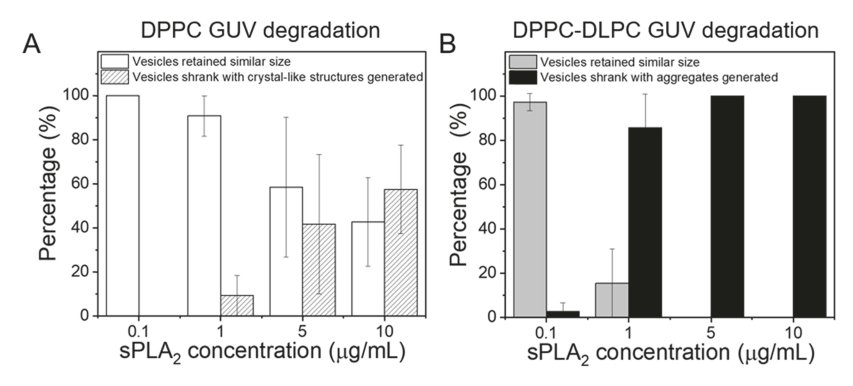


Figure 2. Statistical analysis of degradation results of (A) DPPC GUVs and (B) DPPC-DLPC GUVs ($x_{\text{DLPC}} = 0.63$) as a function of sPLA₂ concentration within 10 min after mixing with sPLA₂ at 23 °C. The percentage shown is the average of the values from at least three independent experimental measurements. In each experiment, at least five vesicles were recorded. The total numbers of DPPC GUVs counted at 0.1, 1, 5, and 10 μ g mL⁻¹ sPLA₂ were 35, 44, 45, and 38, respectively. The numbers of DPPC-DLPC GUVs counted at 0.1 and 1 μ g mL⁻¹ sPLA₂ were 28 and 31, respectively. All the DPPC-DLPC GUVs consistently degraded rapidly after mixing with 5 and 10 μ g mL⁻¹ sPLA₂.

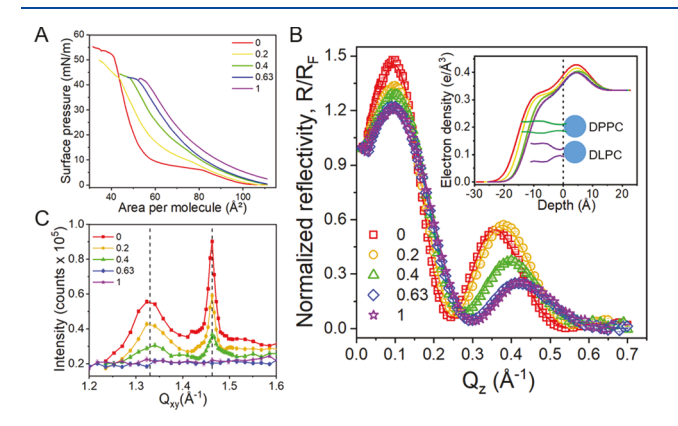


Figure 3. Effects of polyunsaturation on interfacial organization of lipid monolayers. (A) Surface pressure-mean molecular area curves of DPPC, DLPC, and DPPC-DLPC ($x_{DLPC} = 0.2$, 0.4, and 0.63) monolayers at the gas-liquid interface. The legend indicates the molar fractions of DLPC in the monolayers. (B) Normalized reflectivities of DPPC, DLPC, and DPPC-DLPC ($x_{DLPC} = 0.2, 0.4,$ and 0.63) monolayers at 25 mN m⁻¹ at the gas-liquid interface. The structural parameters from fitting the curves are listed in Table 1. The inset presents the electron density profiles across the interface; the same colors are used for the same sets of data. The electron density profiles were aligned at the zero position where lipid tail and head were connected (indicated by the vertical black dashed line). (C) GIXD Bragg peaks of DPPC, DLPC, and DPPC-DLPC ($x_{DLPC} = 0.2$, 0.4, and 0.63) monolayers at 25 mN m⁻¹ at the gas-liquid interface. The baseline of the DPPC and DPPC-DLPC ($x_{\rm DLPC} = 0$, 0.2, and 0.4) monolayers was shifted by -20000 counts to compare the peak positions and relative intensities.

presence of DLPC in the monolayers were also observed when monounsaturated phospholipids were added to saturated phospholipid monolayers. ⁵⁴

To track the lipid molecular packing in more detail, XR and GIXD measurements were conducted on the DPPC, DLPC, and DPPC—DLPC films at the gas—liquid interface. The XR results are presented in Figure 3B, and the corresponding electron density profiles are shown in the inset. The structural parameters from fitting the data are reported in Table 1. Increasing the molar fraction of DLPC progressively thinned the overall films by about 4 Å and lowered the average electron density of tails by about 8% until the molar fraction of DLPC reached 0.63. A further increase of the molar fraction of DLPC in the lipid films beyond 0.63 showed limited effects on the interfacial packing of the films.

GIXD spectra revealed that incorporation of DLPC into DPPC films decreased the Bragg peak intensity, which indicated a decrease in the total surface coverage of the DPPC condensed domains (Figure 3C). The peak positions and widths of the Bragg peaks and Bragg rods of the DPPC and the DPPC-DLPC ($x_{DLPC} = 0.2$ and 0.4) monolayers were similar, suggesting a similar lateral packing structure in the DPPC condensed domains (with the structural parameters listed in Table S2). When the molar fraction of DLPC in the lipid film reached 0.63 at 25 mN m⁻¹, no DPPC condensed domain was detectable at the gas-liquid interface and no further change in the overall packing structure of the film was observed. Similar trends were observed when more DLPC was present in the mixture of DPPC with 1,2-dioleoyl-sn-glycero-3phosphocholine (DOPC) films: smaller condensed phase domains with less total surface coverage appeared when the molar fraction of DOPC in the films was increased. 54,55 The

Table 1. Structural Parameters from Model Fitting of X-ray Reflectivity Curves for DPPC, DLPC, and DPPC-DLPC ($x_{DLPC} = 0.2, 0.4, \text{ and } 0.63$) Monolayers at a Constant Pressure of 25 mN m⁻¹ at the Gas-Liquid Interface^a

$x_{ m DLPC}$	0	0.2	0.4	0.63	1
σ_0 (Å)	$3.5^{+0.1}_{-0.1}$	$3.1^{+0.1}_{-0.1}$	$3.1^{+0.3}_{-0.2}$	$3.3^{+0.3}_{-0.3}$	$3.3^{+0.3}_{-0.4}$
d_{head} (Å)	$8.7^{+0.7}_{-1.4}$	$8.6^{+0.7}_{-1.3}$	$9.5^{+1.2}_{-2.6}$	$8.0^{+1.8}_{-3.0}$	$7.6^{+2.7}_{-2.6}$
$ ho_{ m head}$ (e Å $^{-3}$)	$0.454^{+0.017}_{-0.008}$	$0.433^{+0.013}_{-0.003}$	$0.415^{+0.023}_{-0.007}$	$0.422^{+0.050}_{-0.016}$	$0.425^{+0.046}_{-0.022}$
d_{tail} (Å)	$15.5^{+0.7}_{-0.5}$	$14.4^{+0.6}_{-0.5}$	$12.6^{+1.4}_{-0.7}$	$12.1^{+0.2}_{-1.0}$	$12.1_{-1.3}^{+1.5}$
$ ho_{ m tail}$ (e Å $^{-3}$)	$0.330^{+0.004}_{-0.004}$	$0.320^{+0.004}_{-0.004}$	$0.316^{+0.010}_{-0.007}$	$0.304^{+0.01}_{-0.01}$	$0.305^{+0.012}_{-0.017}$

[&]quot;The electron density of the aqueous phase was 0.334 e Å^{-3} . The error bar of each parameter was calculated based on one standard deviation from the best fitted value.

critical molar fraction of the monounsaturated DOPC, above which no detectable condensed domains appeared, was about 0.7, reasonably higher than that for DLPC. 54,55

Molecular Packing Structures of the Films after sPLA₂-Catalyzed Degradation. The molecular organizations of DPPC, DLPC, and DPPC-DLPC ($x_{\rm DLPC} = 0.2, 0.4$, and 0.63) films after degradation catalyzed by sPLA₂ were also measured by XR and GIXD. For comparison, the GIXD measurements were also conducted on the PA (a degradation product of DPPC) and LA (a degradation product of DLPC) films at a constant pressure of 10 mN m⁻¹, which was similar to the pressure after DPPC film degradation with a constant area. After DPPC degradation, the two Bragg peaks representing the nearest neighbor tilted lateral packing of the DPPC tails were replaced by five new, strong Bragg peaks (Figure 4A). The positions and intensity ratios of these five

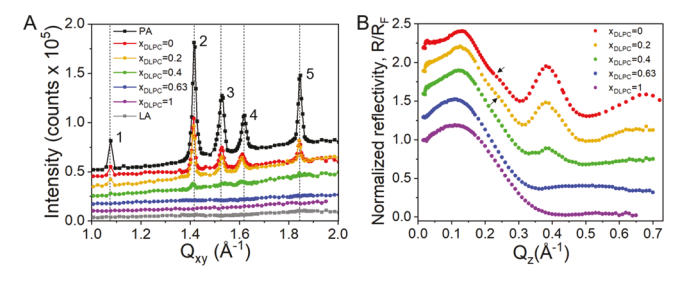


Figure 4. Results of GIXD and XR measurements on lipid films after sPLA₂-catalyzed degradation. (A) GIXD Bragg peaks of degraded DPPC, DPPC–DLPC ($x_{\rm DLPC} = 0.2$, 0.4, and 0.63), and DLPC films. GIXD Bragg peaks of PA and LA films at a constant pressure of 10 mN m⁻¹ on the same Ca²⁺ buffer are also plotted. The vertical dashed lines indicate the peak positions of the five Bragg peaks for the PA film. (B) Normalized X-ray reflectivity curves of degraded DPPC, DPPC–DLPC ($x_{\rm DLPC} = 0.2$, 0.4, and 0.63), and DLPC films. The black arrows indicate the characteristic secondary peaks induced by the presence of PA–Ca²⁺ complex crystal domains. In both figures, data are offset for clarity.

Bragg peaks were similar to those obtained from a pure PA film on a Ca²⁺ buffer. The five Bragg peaks indicated that the film contained stable and highly organized PA-Ca²⁺ crystals generated through degradation. ⁵¹ The Bragg peak intensities obtained from the degraded DPPC film were less than those of a pure PA film because the degraded DPPC film contained another degradation product, 1-palmitoyl-2-hydroxy-sn-glycero-3-phosphocholine, which reduced the total area coverage of the PA-Ca²⁺ complex. For the degraded films of DPPC-DLPC ($x_{DLPC} = 0.2$), the Bragg peak positions and intensities remained similar to those of the degraded DPPC film. When the mole fraction of DLPC was further increased to 0.4, the peaks appeared at the same positions (Table S3), but the intensities of the Bragg peaks decreased significantly, indicating a decrease in the total surface coverage of the ordered domains. Therefore, the degraded DPPC-DLPC films at lower DLPC concentrations ($x_{DLPC} = 0.2$ and 0.4) still contained highly ordered crystal structures of PA-Ca2+ complexes at the interface. With a higher molar fraction of DLPC (0.63 and above), no GIXD Bragg peaks could be detected. The GIXD results for a degraded DLPC film and a pure LA film are presented in Figure 4A, which showed the feature of a fluid monolayer with no detectable in-plane ordered structures. The molecules are loosely packed and disordered at the gas-liquid interface. Therefore, at a high molar fraction (0.63 and above),

degradation products of DLPC disrupted the formation of PA-Ca²⁺ crystals, which was consistent with the discovery of the lack of obvious crystal structures on the DPPC-DLPC GUVs upon degradation (bottom row of Figure 1B).

The PA-Ca²⁺ complex generated ordered multilayer domains at the interface, which induced two features in the XR curve of the degraded DPPC film (Figure 4B): additional secondary peaks (indicated by the black arrows) and less intensity decay along the Q_z direction compared to a typical monolayer. 51 These features remained in the reflectivity curves of the degraded DPPC-DLPC film with $x_{\rm DLPC}$ = 0.2 (the orange dotted lines in Figure 4B). With a further increase of the DLPC molar fraction, these characteristic features became less pronounced. For the degraded DPPC-DLPC film with $x_{\rm DLPC}$ = 0.4, these characteristics were difficult to discern. In the degraded films containing DPPC-DLPC with $x_{DLPC} = 0.63$ or pure DLPC (the blue and purple dotted lines, respectively, in Figure 4B), these features were completely absent from the reflectivity curves. For both cases, the intensity of the second reflectivity peak decreased significantly and all peaks became broader, indicating a substantial decrease in average film thickness.

DISCUSSION

Measurements of the interfacial molecular packing structures of the lipid films before and after lipid degradation using high spatial resolution techniques like XR and GIXD provide a molecular-level explanation for the observed degradation kinetics and morphological evolution of DPPC GUVs and DPPC-DLPC GUVs ($x_{DLPC} = 0.63$) after their exposure to sPLA₂. The presence of a high molar fraction of DLPC (x_{DLPC} = 0.63) in DPPC membranes fundamentally altered the degradation processes of vesicles. After being mixed with a high concentration of sPLA₂ (5 μ g mL⁻¹), most DPPC GUVs shrank and crystal-like structures were generated, which were the PA-Ca²⁺ complexes observed in the GIXD measurements. The continuous loss of lysoPC and formation of PA-Ca²⁺ crystals reduced the lipid surface coverage and induced pore formation on the membranes. 52,56 These pores further promoted membrane degradation and grew continuously to form the defects observed on the membranes. On the other hand, the presence of a high molar fraction of DLPC (x_{DLPC} = 0.63) in DPPC membranes enhanced the degradation rate of the GUVs because the DLPC molecules packed loosely at the interface and increased membrane fluidity, as quantified by lipid film monolayer compression isotherms and X-ray measurements. In addition, during the degradation of DPPC-DLPC GUVs, formation of a large fraction of coneshaped LA molecules without a sufficient time to reorganize may have destabilized and further accelerated the degradation of these GUVs. 1,57 Despite the fact that experimental measurements were conducted at room temperature, the observed phenomena should provide a good indication of interfacial behavior of the lipids and their degradation products within a temperature range (including the physiological temperature) at which the lipids remain in the same phase. The quantification of the molecular packing and interactions at quasi-equilibrium provides a reference for the future study of the film degradation kinetics using grazing-incidence X-ray offspecular scattering. 58,59

Crystal formation after cell membrane lipid degradation was reported to enhance nonspecific lipoprotein adsorption and probably contribute to development of vascular diseases,³³ so

the presence of abundant polyunsaturated phospholipids may provide a mechanism to prevent them. This possibility is supported by the observation that lower percentages of polyunsaturation were found in the aged brain with Alzheimer's disease compared to the normal aged brain 60,61 and that the percentage of polyunsaturation in the retina with advanced age-related macular degeneration was lower than that in the age-matched normal retina.⁶² Although the concentration of DLPC is low in normal brain and retina, most polyunsaturated phospholipids have four or six double carbon bonds in at least one tail, which may be more effective in preventing crystal formation of the degradation products. The results of this study may shed light on one protective function of the abundant polyunsaturated phospholipids present in membranes of the brain and retina where crystal formation is undesirable.

CONCLUSIONS

Observation of GUV degradation using fluorescence microscopy and quantification of lipid interfacial organization before and after lipid degradation using X-ray surface scattering techniques provide tools for optimization of the liposome drug delivery system responding to different local concentrations of sPLA₂. From the results of this study, we may also provide insights into the roles of polyunsaturated phospholipids in biological membranes. Including high molar fractions of polyunsaturated phospholipids affected lipid membrane degradation through two mechanisms: (1) loose and fluidic packing of the phospholipids facilitated enzyme adsorption and promoted faster lipid degradation, and (2) disordered packing of the degradation products disrupted crystal structure formation. It is possible that vesicle degradation can be designed by manipulating the combination of saturated and polyunsaturated phospholipids so as to achieve reasonable vesicle stability and desired drug release schedules.

ASSOCIATED CONTENT

S Supporting Information

The Supporting Information is available free of charge on the ACS Publications website at DOI: 10.1021/acs.langmuir.9b01476.

Molecular structures and degradation catalyzed by sPLA₂, modified electroformation method and its results, observation of GUVs without sPLA₂, exposure times of fluorescence images, and lateral packing structural parameters of lipid films before and after degradation (PDF)

AUTHOR INFORMATION

Corresponding Author

*E-mail: liuying@uic.edu.

ORCID

Pin Zhang: 0000-0003-0107-221X Joseph Kalkowski: 0000-0002-5914-5955 Chang Liu: 0000-0001-5271-9867 Ursula Perez-Salas: 0000-0003-4675-5604

Ying Liu: 0000-0002-1207-8409

Notes

The authors declare no competing financial interest.

ACKNOWLEDGMENTS

The study is partially supported by the National Science Foundation-Nanomanufacturing Program to Y.L. (NSF CAREER #1350731). NSF's ChemMatCARS Sector 15 is principally supported by the Divisions of Chemistry (CHE) and Materials Research (DMR), National Science Foundation, under grant number NSF/CHE-1834750. Use of the Advanced Photon Source, an Office of Science User Facility operated for the U.S. Department of Energy (DOE) Office of Science by Argonne National Laboratory, was supported by the U.S. DOE under Contract No. DE-AC02-06CH11357. The authors thank Professor Mark L. Schlossman for helpful discussions. The authors thank Professor Ka Yee Lee for providing the design of the custom-made trough with a stirring system.

REFERENCES

- (1) Pinot, M.; Vanni, S.; Pagnotta, S.; Lacas-Gervais, S.; Payet, L.-A.; Ferreira, T.; Gautier, R.; Goud, B.; Antonny, B.; Barelli, H. Polyunsaturated phospholipids facilitate membrane deformation and fission by endocytic proteins. *Science* **2014**, *345*, 693–697.
- (2) Stinson, A. M.; Wiegand, R. D.; Anderson, R. E. Fatty acid and molecular species compositions of phospholipids and diacylglycerols from rat retinal membranes. *Exp. Eye Res.* **1991**, *52*, 213–218.
- (3) Miljanich, G. P.; Sklar, L. A.; White, D. L.; Dratz, E. A. Disaturated and dipolyunsaturated phospholipids in the bovine retinal rod outer segment disk membrane. *Biochim. Biophys. Acta* **1979**, 552, 294–306.
- (4) Lambeau, G.; Gelb, M. H. Biochemistry and Physiology of Mammalian Secreted Phospholipases A2. *Annu. Rev. Biochem.* **2008**, 77, 495–520.
- (5) Murakami, M.; Sato, H.; Miki, Y.; Yamamoto, K.; Taketomi, Y. A new era of secreted phospholipase A2. *J. Lipid Res.* **2015**, *56*, 1248–1261.
- (6) Yedgar, S.; Lichtenberg, D.; Schnitzer, E. Inhibition of phospholipase A2 as a therapeutic target. *Biochim. Biophys. Acta* **2000**, *1488*, 182–187.
- (7) Webb, N. R. Secretory phospholipase A2 enzymes in atherogenesis. *Curr. Opin. Lipidol.* **2005**, *16*, 341–344.
- (8) Hui, D. Y. Phospholipase A2 enzymes in metabolic and cardiovascular diseases. *Curr. Opin. Lipidol.* **2012**, 23, 235–240.
- (9) Nevalainen, T. J.; Haapamäki, M. M.; Grönroos, J. M. Roles of secretory phospholipases A2 in inflammatory diseases and trauma. *Biochim. Biophys. Acta* **2000**, *1488*, 83–90.
- (10) Abe, T.; Sakamoto, K.; Kamohara, H.; Hirano, Y. I.; Kuwahara, N.; Ogawa, M. Group II phospholipase A2 is increased in peritoneal and pleural effusions in patients with various types of cancer. *Int. J. Cancer* **1997**, *74*, 245–250.
- (11) Yamashita, S.; Yamashita, J.; Ogawa, M. Overexpression of group II phospholipase A2 in human breast cancer tissues is closely associated with their malignant potency. *Br. J. Cancer* **1994**, *69*, 1166–1170.
- (12) Singh, J.; Ranganathan, R. Quantitation of lysolipids, fatty acids, and phospholipase A2activity and correlation with membrane polarity. *J. Lipid Res.* **2012**, *53*, 1993–2001.
- (13) Vacklin, H. P.; Tiberg, F.; Fragneto, G.; Thomas, R. K. Phospholipase A2Hydrolysis of Supported Phospholipid Bilayers: A Neutron Reflectivity and Ellipsometry Study†. *Biochemistry* **2005**, *44*, 2811–2821.
- (14) Van Blitterswijk, W. J.; Van der Meer, B. W.; Hilkmann, H. Quantitative contributions of cholesterol and the individual classes of phospholipids and their degree of fatty acyl (un)saturation to membrane fluidity measured by fluorescence polarization. *Biochemistry* **2002**, *26*, 1746–1756.
- (15) Niebylski, C. D.; Salem, N. A calorimetric investigation of a series of mixed-chain polyunsaturated phosphatidylcholines: effect of sn-2 chain length and degree of unsaturation. *Biophys. J.* **1994**, *67*, 2387–2393.

(16) Holte, L. L.; Separovic, F.; Gawrisch, K. Nuclear magnetic resonance investigation of hydrocarbon chain packing in bilayers of polyunsaturated phospholipids. *Lipids* **1996**, *31*, S199–S203.

- (17) Mitchell, D. C.; Litman, B. J. Molecular Order and Dynamics in Bilayers Consisting of Highly Polyunsaturated Phospholipids. *Biophys. J.* **1998**, *74*, 879–891.
- (18) Litman, B. J.; Mitchell, D. C. A role for phospholipid polyunsaturation in modulating membrane protein function. *Lipids* **1996**, 31, S193–S197.
- (19) Zerouga, M.; Jenski, L. J.; Stillwell, W. Comparison of phosphatidylcholines containing one or two docosahexaenoic acyl chains on properties of phospholipid monolayers and bilayers. *Biochim. Biophys. Acta* **1995**, *1236*, 266–272.
- (20) Stubbs, C. D.; Smith, A. D. The modification of mammalian membrane polyunsaturated fatty acid composition in relation to membrane fluidity and function. *Biochim. Biophys. Acta* **1984**, 779, 89–137.
- (21) Jarc, E.; Kump, A.; Malavašič, P.; Eichmann, T. O.; Zimmermann, R.; Petan, T. Lipid droplets induced by secreted phospholipase A2 and unsaturated fatty acids protect breast cancer cells from nutrient and lipotoxic stress. *Biochim. Biophys. Acta, Mol.Cell Biol. Lipids* **2018**, *1863*, 247–265.
- (22) Balsinde, J.; Winstead, M. V.; Dennis, E. A. Phospholipase A2regulation of arachidonic acid mobilization. *FEBS Lett.* **2002**, *531*, 2–6.
- (23) Rapoport, S. I.; Taha, A. Imaging Brain DHA Metabolism in Vivo, in Animals, and Humans. In *Omega-3 Fatty Acids in Brain and Neurological Health*; Watson, R. R.; De Meester, F., Eds.; Academic Press: Boston, 2014; pp 265–275.
- (24) Tapiero, H.; Nguyen Ba, G.; Couvreur, P.; Tew, K. D. Polyunsaturated fatty acids (PUFA) and eicosanoids in human health and pathologies. *Biomed. Pharmacother.* **2002**, *56*, 215–222.
- (25) Connor, W. E. Importance of n-3 fatty acids in health and disease. *Am. J. Clin. Nutr.* **2000**, *71*, 171S-175S.
- (26) Leslie, C. C. Regulation of arachidonic acid availability for eicosanoid production. *Biochem. Cell Biol.* **2004**, 82, 1–17.
- (27) Jørgensen, K.; Davidsen, J.; Mouritsen, O. G. Biophysical mechanisms of phospholipase A2 activation and their use in liposome-based drug delivery. *FEBS Lett.* **2002**, *531*, 23–27.
- (28) Donovan, A. J.; Kalkowski, J.; Szymusiak, M.; Wang, C.; Smith, S. A.; Klie, R. F.; Morrissey, J. H.; Liu, Y. Artificial dense granules: a procoagulant liposomal formulation modeled after platelet polyphosphate storage pools. *Biomacromolecules* **2016**, *17*, 2572–2581.
- (29) Donovan, A. J.; Kalkowski, J.; Smith, S. A.; Morrissey, J. H.; Liu, Y. Size-controlled synthesis of granular polyphosphate nanoparticles at physiologic salt concentrations for blood clotting. *Biomacromolecules* **2014**, *15*, 3976–3984.
- (30) Pourhassan, H.; Clergeaud, G.; Hansen, A. E.; Østrem, R. G.; Fliedner, F. P.; Melander, F.; Nielsen, O. L.; O'Sullivan, C. K.; Kjær, A.; Andresen, T. L. Revisiting the use of sPLA2-sensitive liposomes in cancer therapy. *J. Controlled Release* **2017**, *261*, 163–173.
- (31) Chonn, A.; Cullis, P. R.; Devine, D. V. The role of surface charge in the activation of the classical and alternative pathways of complement by liposomes. *J. Immunol.* **1991**, *146*, 4234–4241.
- (32) Seelig, A.; Seelig, J. Effect of a single cis double bond on the structure of a phospholipid bilayer. *Biochemistry* **1977**, *16*, 45–50.
- (33) Hong, C. Y.; Han, C.-T.; Chao, L. Nonspecific Binding Domains in Lipid Membranes Induced by Phospholipase A2. *Langmuir* **2016**, 32, 6991–6999.
- (34) Dawson, R. M. C.; Irvine, R. F.; Bray, J.; Quinn, P. J. Long-chain unsaturated diacylglycerols cause A perturbation in the structure of phospholipid bilayers rendering them susceptible to phospholipase attack. *Biochem. Biophys. Res. Commun.* 1984, 125, 836–842.
- (35) Balashev, K.; Atanasov, V.; Mitewa, M.; Petrova, S.; Bjørnholm, T. Kinetics of degradation of dipalmitoylphosphatidylcholine (DPPC) bilayers as a result of vipoxin phospholipase A2 activity: An atomic force microscopy (AFM) approach. *Biochim. Biophys. Acta, Biomembr.* **2011**, *1808*, 191–198.

(36) Dahmen-Levison, U.; Brezesinski, G.; Möhwald, H. Specific adsorption of PLA2 at monolayers. *Thin Solid Films* **1998**, 327-329, 616-620.

- (37) De Tullio, L.; Fanani, M. L.; Maggio, B. Surface mixing of products and substrate of PLA2 in enzyme-free mixed monolayers reproduces enzyme-driven structural topography. *Biochim. Biophys. Acta, Biomembr.* **2013**, *1828*, 2056–2063.
- (38) Li, J.; Chen, Z.; Wang, X.; Brezesinski, G.; Möhwald, H. Dynamic observations of the hydrolysis of a DPPC monolayer at the air/water interface catalyzed by phospholipase A2. *Angew. Chem. Int. Ed.* **2000**, 39, 3059–3062.
- (39) McConlogue, C. W.; Vanderlick, T. K. A close look at domain formation in DPPC monolayers. *Langmuir* **1997**, *13*, 7158–7164.
- (40) Sanchez, S. A.; Bagatolli, L. A.; Gratton, E.; Hazlett, T. L. A two-photon view of an enzyme at work: Crotalus atrox venom PLA 2 interaction with single-lipid and mixed-lipid giant unilamellar vesicles. *Biophys. J.* **2002**, *82*, 2232–2243.
- (41) Zhai, X.; Li, J.; Brezesinski, G.; He, Q.; Möhwald, H.; Lai, L.; Liu, Y.; Liu, L.; Gao, Y. Direct Observations of the Cleavage Reaction of an L-DPPC Monolayer Catalyzed by Phospholipase A2 and Inhibited by an Indole Inhibitor at the Air/Water Interface. *ChemBioChem* **2003**, *4*, 299–305.
- (42) Salem, N., Jr; Pawlosky, R.; Wegher, B.; Hibbeln, J. In vivo conversion of linoleic acid to arachidonic acid in human adults. *Prostaglandins, Leukotrienes Essent. Fatty Acids* **1999**, *60*, 407–410.
- (43) Angelova, M.; Soléau, S.; Méléard, P.; Faucon, F.; Bothorel, P. Preparation of giant vesicles by external AC electric fields. Kinetics and applications. In *Trends in Colloid and Interface Science VI*; Springer: 1992; pp 127–131.
- (44) Angelova, M. I.; Dimitrov, D. S. Liposome electroformation. Faraday Discuss. Chem. Soc. 1986, 81, 303–311.
- (45) Estes, D. J.; Mayer, M. Electroformation of giant liposomes from spin-coated films of lipids. *Colloids Surf., B* **2005**, *42*, 115–123.
- (46) Dutta, P. Studies of monolayers using synchrotron X-ray diffraction. Curr. Opin. Solid State Mater. Sci. 1997, 2, 557–562.
- (47) Dutta, P.; Peng, J. B.; Lin, B.; Ketterson, J. B.; Prakash, M.; Georgopoulos, P.; Ehrlich, S. X-Ray Diffraction Studies of Organic Monolayers on the Surface of Water. *Phys. Rev. Lett.* **1987**, *58*, 2228–2231.
- (48) Kjaer, K.; Als-Nielsen, J.; Helm, C. A.; Laxhuber, L. A.; Möhwald, H. Ordering in Lipid Monolayers Studied by Synchrotron X-Ray Diffraction and Fluorescence Microscopy. *Phys. Rev. Lett.* **1987**, 58, 2224–2227.
- (49) Parratt, L. G. Surface studies of solids by total reflection of X-rays. *Phys. Rev.* **1954**, *95*, 359–369.
- (50) Bu, W.; Vaknin, D. Bilayer and Trilayer Crystalline Formation by Collapsing Behenic Acid Monolayers at Gas/Aqueous Interfaces. *Langmuir* **2008**, *24*, 441–447.
- (51) Zhang, P.; Villanueva, V.; Kalkowski, J.; Liu, C.; Donovan, A. J.; Bu, W.; Schlossman, M. L.; Lin, B.; Liu, Y. Molecular interactions of phospholipid monolayers with a model phospholipase. *Soft Matter* **2019**, *15*, 4068–4077.
- (52) Wacklin, H. P.; Tiberg, F.; Fragneto, G.; Thomas, R. K. Distribution of reaction products in phospholipase A2 hydrolysis. *Biochim. Biophys. Acta, Biomembr.* **2007**, *1768*, 1036–1049.
- (53) Kaganer, V. M.; Möhwald, H.; Dutta, P. Structure and phase transitions in Langmuir monolayers. *Rev. Mod. Phys.* **1999**, *71*, 779–819.
- (54) Nag, K.; Keough, K. M. Epifluorescence microscopic studies of monolayers containing mixtures of dioleoyl- and dipalmitoylphosphatidylcholines. *Biophys. J.* **1993**, *65*, 1019–1026.
- (55) Suga, K.; Umakoshi, H. Detection of Nanosized Ordered Domains in DOPC/DPPC and DOPC/Ch Binary Lipid Mixture Systems of Large Unilamellar Vesicles Using a TEMPO Quenching Method. *Langmuir* **2013**, *29*, 4830–4838.
- (56) Agafonov, A. V.; Gritsenko, E. N.; Shlyapnikova, E. A.; Kharakoz, D. P.; Belosludtseva, N. V.; Lezhnev, E. I.; Saris, N.-E. L.; Mironova, G. D. Ca2+-Induced Phase Separation in the Membrane of

Palmitate-Containing Liposomes and Its Possible Relation to Membrane Permeabilization. *J. Membr. Biol.* **2007**, *215*, 57–68.

- (57) Belosludtsev, K. N.; Belosludtseva, N. V.; Agafonov, A. V.; Astashev, M. E.; Kazakov, A. S.; Saris, N.-E. L.; Mironova, G. D. Ca2+—dependent permeabilization of mitochondria and liposomes by palmitic and oleic acids: A comparative study. *Biochim. Biophys. Acta, Biomembr.* **2014**, *1838*, 2600–2606.
- (58) Dai, Y.; Lin, B.; Meron, M.; Kim, K.; Leahy, B.; Shpyrko, O. G. A comparative study of Langmuir surfactant films: Grazing incidence x-ray off-specular scattering vs. x-ray specular reflectivity. *J. Appl. Phys.* **2011**, *110*, 102213.
- (59) Dai, Y.; Lin, B.; Meron, M.; Kim, K.; Leahy, B.; Witten, T. A.; Shpyrko, O. G. Synchrotron X-ray Studies of Rapidly Evolving Morphology of Self-Assembled Nanoparticle Films under Lateral Compression. *Langmuir* **2013**, *29*, 14050–14056.
- (60) Söderberg, M.; Edlund, C.; Kristensson, K.; Dallner, G. Fatty acid composition of brain phospholipids in aging and in Alzheimer's disease. *Lipids* **1991**, *26*, 421–425.
- (61) Svennerholm, L. Distribution and fatty acid composition of phosphoglycerides in normal human brain. *J. Lipid Res.* **1968**, *9*, 570–579
- (62) van Kuijk, F. J.; Buck, P. Fatty acid composition of the human macula and peripheral retina. *Invest. Ophthalmol. Visual Sci.* **1992**, *33*, 3493–3496.